Density Functional Theory Calculations of Dense TiO_2 Polymorphs: Implication for Visible-Light-Responsive Photocatalysts

Ming-Yu Kuo,[†] Cheng-Lung Chen,*[,‡] Chih-Yu Hua,[‡] Hsiao-Ching Yang,[‡] and Pouyan Shen[†]

Institute of Materials Science and Engineering and Department of Chemistry, National Sun Yat-sen University, Kaohsiung, Taiwan, Republic of China

Received: March 3, 2005

Structural parameters and electronic band gaps of dense TiO_2 polymorphs, i.e., α-PbO_2, baddeleyite, fluorite, and cotunnite types of structures, were calculated using a first-principles density functional method with local-density approximation. The ambient phases, i.e., rutile and anatase, with known theoretical and experimental data were used to ensure the validity of the calculations. The fluorite-type TiO_2 turned out to have the narrowest band gap, 1.08 or 2.18 eV after applying a very approximate band gap correction, due to highly symmetrical TiO_8 polyhedra with Ti_{3d} and O_{2p} orbitals in the most mixed state. Ti with eight coordinated oxygens, as feasible under high pressure or residual stress, may have potential applications as a visible-light-responsive photocatalyst.

I. Introduction

The discovery of the photocatalytic splitting of water on titania (TiO_2) electrodes[1] has encouraged extensive studies of colloidal TiO_2 particles focusing on the photocatalysis of the ambient phases, i.e., anatase and rutile, with Ti with a coordination number (CN) of 6. The promising applications include energy renewal/storage[2] and the total destruction of organic compounds in polluted air/waters.[3] With a rather wide band gap, the ambient TiO_2 phases are solely responsive to ultraviolet light. It is therefore of great interest to find out whether a specific dense polymorph of TiO_2 has a narrow band gap for potential photocatalytic applications under visible light.

There are a number of high-pressure TiO_2 polymorphs,[4−11] having zero-pressure densities (ρ_0) greater than rutile ($\rho_0 = 4.13$ g/cm^3), as compiled in Table 1 and Figure 1. The α-PbO_2-type structure (space group *Pbcn*) with Ti still in CN 6 is about 3% denser than rutile.[7] The baddeleyite ($P2_1/c$),[8−9] fluorite ($Fm3m$),[10] and cotunnite types ($Pnma$)[11] of structures with CN 7, 8, and 9, respectively, are stable at further increasing pressures as indicated by experimental and/or theoretical studies. The post-rutile phases have never been reported to occur in nature until a recent discovery of α-PbO_2-type TiO_2 in ultrahigh-pressure metamorphic rock.[12]

Previous theoretical calculations of the structural parameters and electronic/optical properties of TiO_2 are restricted to ambient phases. The results of these calculations, using various methods such as the full-potential linearized muffin-tin orbital (FPLMTO),[13] empirical tight-binding,[14] cluster,[15] ab initio soft-core pseudopotentials with local-density approximation (LDA),[16] and a first-principles self-consistent linear combination of atomic orbitals via Hartree−Fock (LCAO-HF),[6] generally agree with the experimental results.[17−21] Here, we used first-principles calculations to determine the minimum-energy lattice parameters and band structures of the dense TiO_2 polymorphs. We focused on the specific crystal symmetry and CN that cause extensive mixing of the Ti_{3d} and O_{2p} orbitals for a narrow band gap.

TABLE 1: Zero-Pressure Densities of TiO_2 Polymorphs

polymorphs	structure	g/cm^3
anatase[a]	tetragonal ($I4_1/amd$)	3.79
brookite[b]	orthorhombic ($Pbca$)	3.99
rutile[a]	tetragonal ($P4_2/mnm$)	4.13
rutile[c]	tetragonal ($P4_2/mnm$)	4.25
α-PbO_2 type[d]	orthorhombic ($Pbcn$)	4.33
baddeleyite[e]	monoclinic ($P2_1/c$)	4.73[f]
fluorite[g]	cubic ($Fm3m$)	4.71
cotunnite[h]	orthorhombic ($Pnma$)	5.76

[a] Reference 4. [b] Reference 5. [c] Reference 6. [d] Reference 7. [e] References 8 and 9. [f] Measured at 20 GPa. [g] Reference 10. [h] Calculated from ref 11.

II. Computational Methods

The present calculations were based on the plane-wave pseudopotential and LDA. Electron−core interactions are described by *ultrasoft* pseudopotentials.[22] (The valence states are 2s and 2p shells for O with 6 valence electrons and 3s, 3p, 3d, and 4s states for Ti with 12 valence electrons.) The smooth part of the wave functions was expanded in plane wave with a kinetic-energy cutoff of 340 eV. A $4 \times 4 \times 2$ mesh of k points was used to sample the Brillouin zone for anatase and a $4 \times 4 \times 4$ mesh of k points for other TiO_2 polymorphs. Structural optimizations were carried out by the Broyden−Flecher−Goldfarb−Shanno minimization algorithm. The convergence of displacement was set to less than 0.002 Å, and the energy difference was set to less than 2×10^{-5} eV/atom. All calculations were performed by the software CASTEP.[23]

III. Results

A. Structural Parameters. The calculated lattice parameters a, b, c and the internal parameter u for rutile, anatase, and α-PbO_2-type TiO_2 having cation CN 6 are listed in Table 2.[24−31] These structural parameters agree, within a few percent, with the experimental results[24,29,30] and other ab initio calcula-

* Author to whom correspondence should be addressed. E-mail: chen1@mail.nsysu.edu.tw.
[†] Institute of Materials Science and Engineering.
[‡] Department of Chemistry.

10.1021/jp0510903 CCC: $30.25
Published on Web 04/02/2005

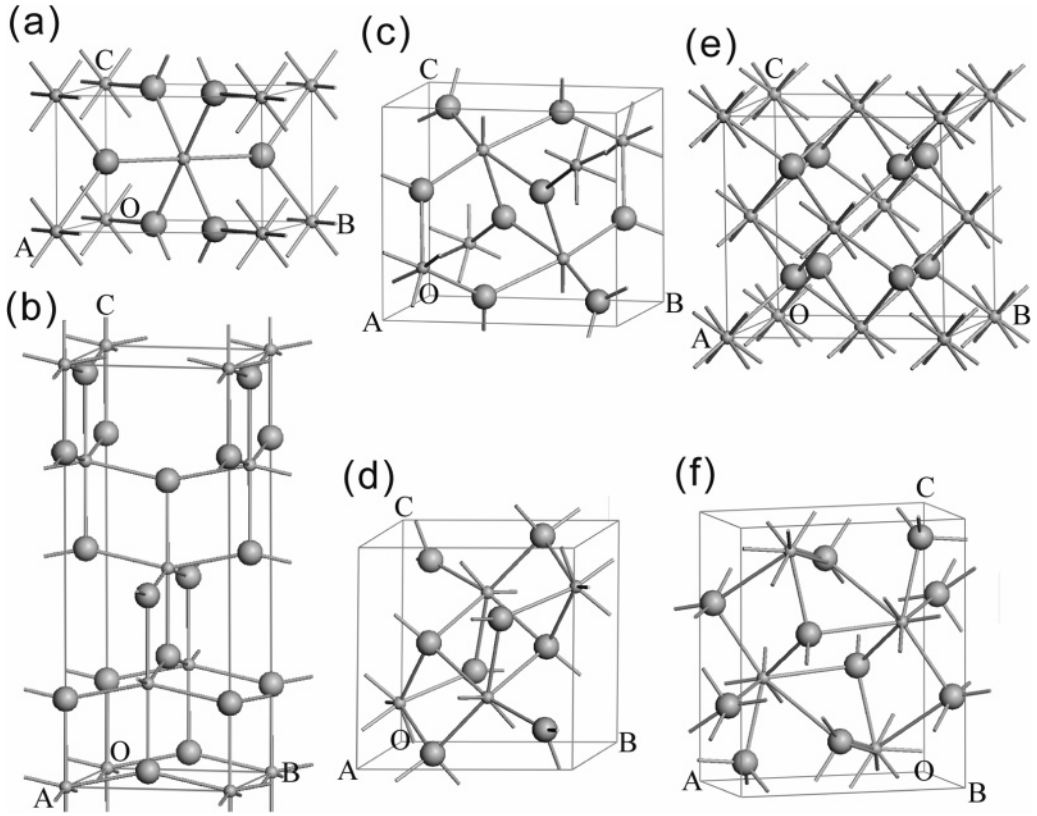

Figure 1. Unit cells of various TiO_2 polymorphs: (a) rutile, (b) anatase, (c) α-PbO_2-type, (d) baddeleyite-type, (e) fluorite-type, (f) cotunnite-type. Large spheres represent the O ions, small spheres the Ti ions, O, A, B, and C denote the origin, *a*-, *b*-, and *c*-axes, respectively.

TABLE 2: Theoretical and Experimental Structural Parameters for Rutile, Anatase, and α-PbO_2 Types of TiO_2[a]

method	*a* (Å)	*b* (Å)	*c* (Å)	*u*
		Rutile		
LDA (this work)	**4.572 (−0.45)**	**4.572 (−0.45)**	**2.926 (−1.12)**	**0.304 (−0.33)**
exptl[b]	**4.593**	**4.593**	**2.959**	**0.305**
PW-LDA[c]	4.555 (−0.83)	4.555 (−0.83)	2.922 (−1.25)	0.304 (−0.33)
PW-LDA[d]	4.567 (−0.57)	4.567 (−0.57)	2.932 (−0.91)	0.305 (0.00)
PW-LDA[e]	4.546 (−1.02)	4.546 (−1.02)	2.925 (−1.15)	not given
PW-LDA[f]	4.574 (−0.41)	4.574 (−0.41)	2.927 (−1.08)	0.304 (−0.33)
		Anatase		
LDA (this work)	**3.740 (−1.11)**	**3.740 (−1.11)**	**9.548 (+0.48)**	**0.207 (−0.48)**
exptl[b]	**3.782**	**3.782**	**9.502**	**0.208**
PW-LDA[c]	3.744 (−1.00)	3.744 (−1.00)	9.497 (−0.05)	0.207 (−0.48)
PW-LDA[e]	3.735 (−1.24)	3.735 (−1.24)	9.534 (+0.34)	not given
PW-LDA[f]	3.758 (−0.63)	3.758 (−0.63)	9.495 (−0.07)	0.208 (0.00)
		α-PbO_2-Type		
LDA (this work)	**4.535 (−0.13)**[g]	**5.447 (−0.84)**[g]	**4.858 (−0.98)**[g]	**0.174 (+1.75)**[g]
exptl[h]	**4.610**	**5.430**	**4.870**	**0.171**
exptl[i]	**4.541**	**5.493**	**4.906**	**0.171**
PW-LDA[j]	4.569 (+0.62)	5.481 (−0.22)	4.929 (+0.47)	0.174 (+1.75)
PW-LDA[f]	4.528 (−0.29)	5.438 (−1.00)	4.954 (+0.98)	0.170 (−0.58)

[a] Numbers in parentheses indicate the percent deviation from the experimental values. [b] Reference 24. [c] Reference 25. [d] Reference 26. [e] Reference 27. [f] Reference 28. [g] The deviation of the α-PbO_2-type TiO_2 is based on ref 29. [h] Reference 30. [i] Reference 29. [j] Reference 31.

tions.[25,28,31] Anatase depicted as a conventional cell in Figure 1b was transformed to a primitive cell (as for other polymorphs) in the present calculation by the software CASTEP,[23] and the lattice parameters agree within 1% with the previous calculation[25] (cf. Table 2).

The calculated lattice parameters of the dense TiO_2 phases with higher CNs (>6), i.e., baddeleyite, fluorite, and cotunnite types of structures, are compiled in Table 3. The resultant structural parameters for baddeleyite and fluorite types of TiO_2 are generally in agreement with other computational[28] and/or experimental data.[11,32] (In general, the computed lattice constants using density functional theory (DFT) LDA are 1−2% smaller than experimental values.) However, the present LDA gave larger lattice constants than the experimental data[11] for cotunnite-type TiO_2 (Table 3) because the former is a minimum-energy calculation value whereas the latter was determined in situ at 61 GPa.[11] (This high-pressure phase is hardly quenchable to ambient pressure unless in liquid nitrogen.[11]) The internal coordinates for the polymorphs were also compiled in Table 3.

The calculated minimum-energy lattice parameters for all of the TiO_2 polymorphs indicate that they are stable at specific cell volume, the dense crystal structure being stable at high pressure and metastable at zero pressure with a positive elastic constant. In fact, the LDA calculated bulk moduli are 178 ± 8,

TABLE 3: Theoretical and Experimental Structural Parameters for Baddeleyite, Fluorite, and Cotunnite Types of TiO_2[a]

method	a (Å)	b (Å)	c (Å)	β (deg)		internal coordinates x	y	z
				Baddeleyite				
LDA (this work)	4.719	4.857	4.958	99.72	Ti	0.279	0.053	0.213
					O1	0.068	0.334	0.341
					O2	0.442	0.760	0.473
expl[b]	4.65	4.93	4.96	99.31	Ti	0.279	0.047	0.209
					O1	0.078	0.354	0.329
					O2	0.444	0.761	0.485
				Fluorite				
LDA (this work)	4.749	4.749	4.749	90	Ti	0	0	0
					O	0.25	0.25	0.25
PW-LDA[c]	4.748	4.748	4.748	90	Ti	0	0	0
					O	0.25	0.25	0.25
				Cotunnite				
LDA (this work)	5.204	3.046	6.067	90	Ti	0.244	0.25	0.116
					O1	0.36	0.25	0.426
					O2	0.025	0.75	0.341
expl[d]	5.163	2.989	5.966	90	Ti	0.264	0.25	0.11
					O1	0.346	0.25	0.422
					O2	0.012	0.75	0.325

[a] Numbers in Parentheses indicate the percent deviation from the experimental results. [b] Measured at ambient pressure, ref 32. [c] Reference 28. [d] The sample was synthesized in an electrically heated diamond anvil cell at 61 GPa and 1100 K and then temperature-quenched to 290 K, ref 11.

214 ± 8, 231 ± 2, 266 ± 5, and 275 ± 6 GPa for anatase, rutile, and dense TiO_2 with α-PbO_2, fluorite, and cotunnite types of structures, respectively, in accordance with less compressibility for a denser phase. Previous calculations on cotunnite-type TiO_2, the hardest known oxide, predicted a remarkably high bulk modulus value for this phase: 380 ± 20 GPa by LCAO-HF and 386 ± 10 GPa by FPLMTO calculation.[11] The experimentally determined bulk modulus for cotunnite-type TiO_2 is even higher, 431 ± 10 GPa,[11] i.e., more than a 10% underestimation of the bulk modulus by their calculations. The bulk moduli calculated in this study for all of the TiO_2 polymorphs may also underestimate experiment by more than 10%.

B. Electronic Properties. *TiO_2 Polymorphs with a Cation Coordination Number of 6.* The band structures of rutile, anatase, and α-PbO_2-type TiO_2 (Figures 2a, 2b, and 2c, respectively) were calculated using the experimental or calculated structure parameters listed in Table 2. The band gaps of other calculations[6,16,25] and experimental results[21,33−38] are also summarized in Table 4.

The band structure of rutile (Figure 2a) was constructed along the high-symmetry direction of the irreducible Brillouin zone (BZ) using the calculated lattice parameters. The corresponding density of state (DOS) and partial density of state (PDOS) in Figure 3a indicated that the band gap 1.86 eV is direct at G. This value is consistent with other calculations[6,16,25] but is smaller than the experimental results (band gap = 3.0 eV).[33,34] (It is generally accepted that LDA calculation tends to underestimate the band gap for insulators and semiconductors.[39]) The band approximately 2.08 eV wide near −16.0 eV resulted from a predominant O_{2s} character. The upper valence band (VB) with a width of 5.95 eV can be attributed to O_{2p} states hybridized with Ti_{3d} character. The widths of the two bands (2.08 and 5.95 eV) are close to the experimental values 1.9 and 5.4 eV, respectively.[36] The separation between the O_{2s} valence states and the minimum of the conduction band (CB) at G turned out to be 17.82 eV, consistent with the Auger spectroscopy results (16−18 eV)[21] and other calculations (e.g., 17.0 eV[16] and 17.98 eV[6]). The lowest CBs are mainly from Ti_{3d} orbitals, which are split into t_{2g}-like (the lower six bands) and e_g-like subbands (the upper four bands), as described by Sorantin and Schwarz for rutile.[40] The topologies of the band structure of rutile are flat, as expected for most ionic compounds. The partial DOS also indicates a substantial degree of hybridization between O_{2p} and Ti_{3d} in the CB region as a result of strong interaction between Ti and O atoms.

TABLE 4: Calculated Band Structures for Rutile, Anatase, and α-PbO_2 Types of TiO_2[a]

	rutile	anatase	α-PbO_2-type
	Band Gap		
LDA (this work)	1.82 (D),[b] 1.86 (D)[c]	2.13 (ID)[c]	2.33 (D),[b] 2.62 (ID)[c]
exptl	3.0[d]	3.2[e]	
LCAO	1.78 (D)[f]	2.04 (ID)[f]	
PW-LDA	2.0 (D),[g] 1.84 (ID)[h]	2.05 (ID)[h]	
	Upper VB Width		
LDA (this work)	5.86,[b] 5.95[c]	4.86[c]	5.38,[b] 5.26[c]
exptl	5.4,[i] 5−6[j]	4.75[k]	
LCAO	6.22[f]	5.17[f]	
PW-LDA	5.7,[g] 6.0[h]	5.0[h]	
	O_{2s} Bandwidth		
LDA (this work)	2.00,[b] 2.08[c]	1.88[c]	2.11,[b] 2.11[c]
exptl	1.9[i]		
LCAO	1.94[f]	1.76[f]	
PW-LDA	1.8[g]		
	Gap between O_{2s} Band and CB		
LDA (this work)	17.76,[b] 17.82[c]	17.71[c]	18.11,[b] 18.26[c]
exptl	16−18[l]		
LCAO	17.98[f]	17.88[f]	
PW-LDA	17.0[g]		

[a] D is the direct band gap. ID is the indirect band bap. Units are in eV. [b] Calculated by using the experimental lattice parameters in Table 2. For α-PbO_2-type TiO_2, the ambient lattice parameters of ref 30 were used. [c] Calculated by using the calculated lattice parameters of this work in Table 2. [d] References 33 and 34. [e] Reference 35. [f] Reference 6. [g] Reference 16. [h] Reference 25. [i] Reference 36. [j] Reference 37. [k] Reference 38. [l] Reference 21.

The calculated band structure of anatase (Figure 2b) shows a minimum band gap of 2.13 eV, which is indirect from the top of the VB near M (point $2\pi/a(0.43, 0.43, 0.0)$ in the BZ) to the bottom of the CB at G. This band gap is in fair agreement with other calculations (e.g., 2.04 eV[6] and 2.05 eV[25]) but is smaller than the experimental results (3.2 eV).[35] In comparison with rutile, anatase is 10% wider in band gap based on either the experimental[33−35] or LDA calculation results.[25] However, the theoretical band gaps are narrower than experimental values for both phases. This indicated that the LDA calculation gives a systematic underestimation of the band gap. Thus, the systematic error being taken into account, the calculation of the band gap is meaningful for the ambient as well as dense TiO_2 polymorphs having no experimental band-gap value available as addressed later. Figure 3b and Table 4 showed that the calculated upper VB width for anatase is 4.86 eV, in fair agreement with the experimental value of 4.75 eV.[38] The calculated O_{2s} bandwidth is 1.88 eV in agreement with other calculations (cf. Table 4), and the band is 17.71 eV below the CB minimum.

The electronic properties of α-PbO_2-type TiO_2 have not been determined theoretically or experimentally. The first such calculation in this study (Table 4) was based on the theoretical and experimental lattice parameters of α-PbO_2-type TiO_2. The band structure (Figure 2c) and corresponding DOS/PDOS (Figure 3c) were shown representatively for the case using theoretical ambient lattice parameters ($a = 4.535$ Å, $b = 5.447$ Å, $c = 4.858$ Å). There is an indirect band gap 2.62 eV from G to Z (Figure 2c). The upper VB and the lower O_{2s} are 5.26

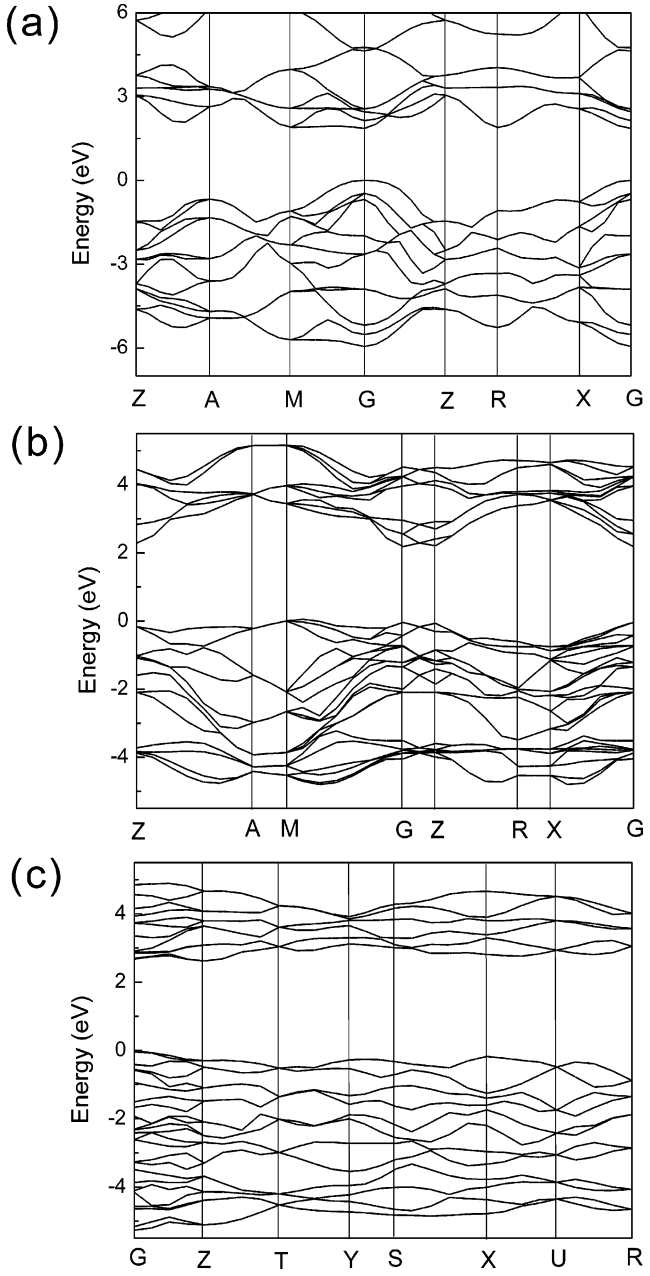

Figure 2. Calculated energy band structures: (a) rutile, (b) anatase, (c) α-PbO_2-type TiO_2.

and 2.11 eV in width, respectively (Figure 3c). The separation between the O_{2s} valence states and the minimum of the CB is approximately 18.26 eV. However, the direct band gaps of 2.33 eV (Table 4) and 2.39 eV were obtained for α-PbO_2 type TiO_2 when calculated, respectively, from the two sets of experimental lattice parameters at ambient pressure, i.e., $a = 4.61$ Å, $b = 5.43$ Å, $c = 4.87$ Å[30] and $a = 4.541$ Å, $b = 5.493$ Å, $c = 4.906$ Å.[29] In any case, the calculated band gap is larger for α-PbO_2-type TiO_2 than those of rutile and anatase.

TiO_2 Polymorphs with the Cation Exceeding 6-Fold Coordination. The band structures of baddeleyite, fluorite, and cotunnite types of TiO_2 (Figures 4a, 4b, and 4c, respectively) were calculated using the experimental or calculated structure parameters listed in Table 3. The detailed values of the band gap are also compiled in Table 5.

The band structure of baddeleyite-type TiO_2 shows an indirect band gap of 2.15 eV from G to B (Figure 4a) as constructed using the calculated lattice parameters $a = 4.719$ Å, $b = 4.857$ Å, $c = 4.958$ Å, $\beta = 99.72°$. The corresponding DOS and PDOS in Figure 5a indicated that the upper VB and the lower O_{2s} are 6.17 and 2.62 eV in width, respectively. The separation between the O_{2s} valence states and the minimum of the CB was found to be approximately 18.11 eV. An additional calculation using experimental lattice parameters ($a = 4.65$ Å, $b = 4.93$ Å, $c = 4.96$ Å, $\beta = 99.31°$) gives a similar indirect band gap of 2.06 eV for baddeleyite-type TiO_2.

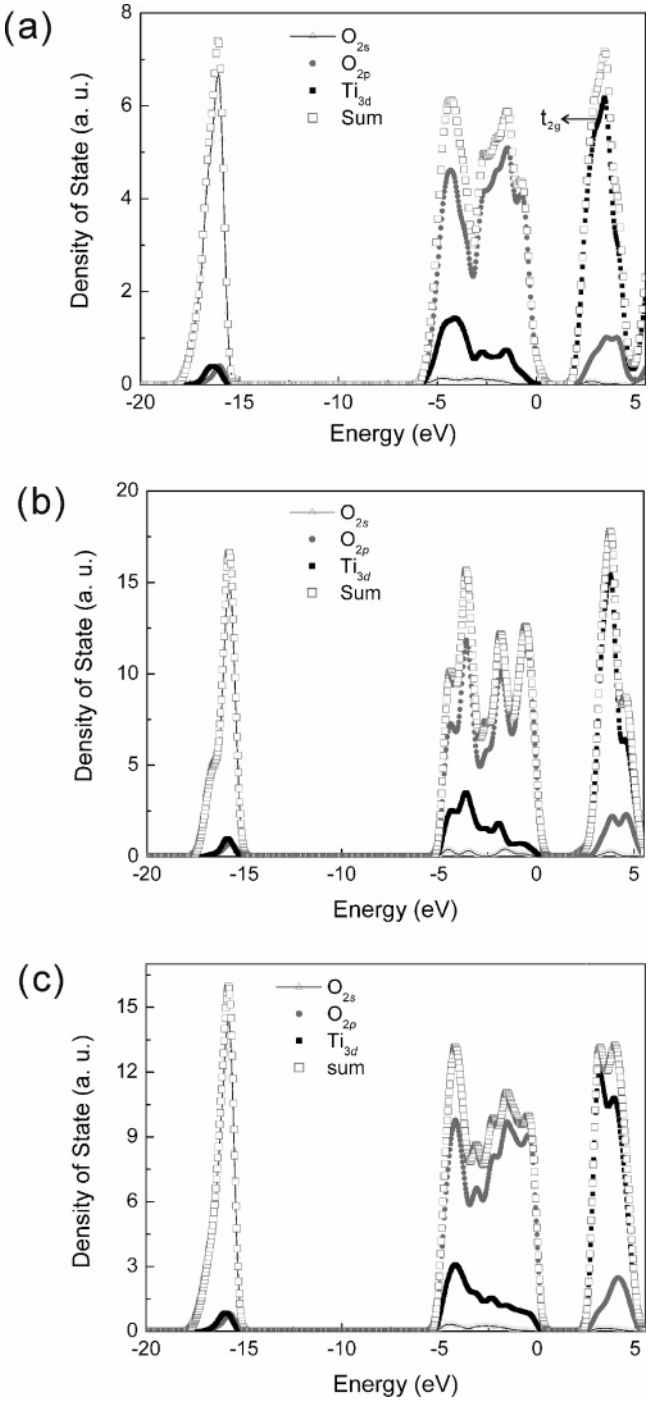

Figure 3. Total and partial DOS: (a) rutile, (b) anatase, (c) α-PbO_2-type TiO_2.

The calculated band structure of fluorite-type TiO_2 using the calculated lattice parameters of 4.749 Å at ambient pressure shows a direct band gap of 1.08 eV (Figure 4b). By contrast, an independent DFT-LDA calculation using the full-potential linearized augmented plane-wave (APW) method,[41] gives a direct band gap, 1.79 eV, and an indirect band gap, 1.04 eV,

TABLE 5: Calculated Band Structures for Baddeleyite, Fluorite, and Cotunnite Types of TiO_2[a]

	baddeleyite	fluorite	cotunnite
band gap	2.06 (ID),[b] 2.15(ID)[c]	1.08[c](D)	1.65(D),[b] 1.72(D)[c]
upper VB width	6.19,[b] 6.17[c]	7.54[c]	7.35,[b] 6.94[c]
O_{2s} bandwidth	2.64,[b] 2.62[c]	4.18[c]	4.13,[b] 3.64[c]
gap between O_{2s} band and CB	18.08,[b] 18.11[c]	16.60[c]	17.63,[b] 17.81[c]

[a] D is the direct band gap. ID is the indirect band gap. Units are in eV. [b] Calculated by using the experimental lattice parameters in Table 3. [c] Calculated by using the calculated lattice parameters of this work in Table 3.

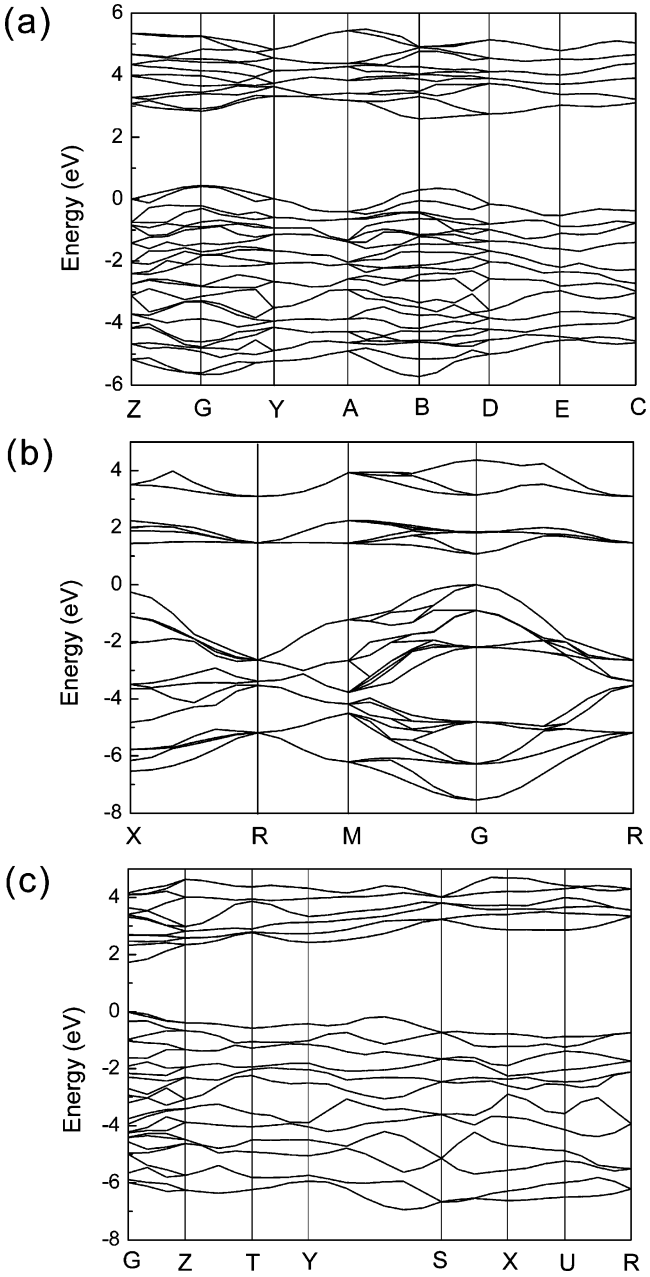

Figure 4. Calculated energy band structures: (a) baddeleyite-, (b) fluorite-, (c) cotunnite-type TiO_2.

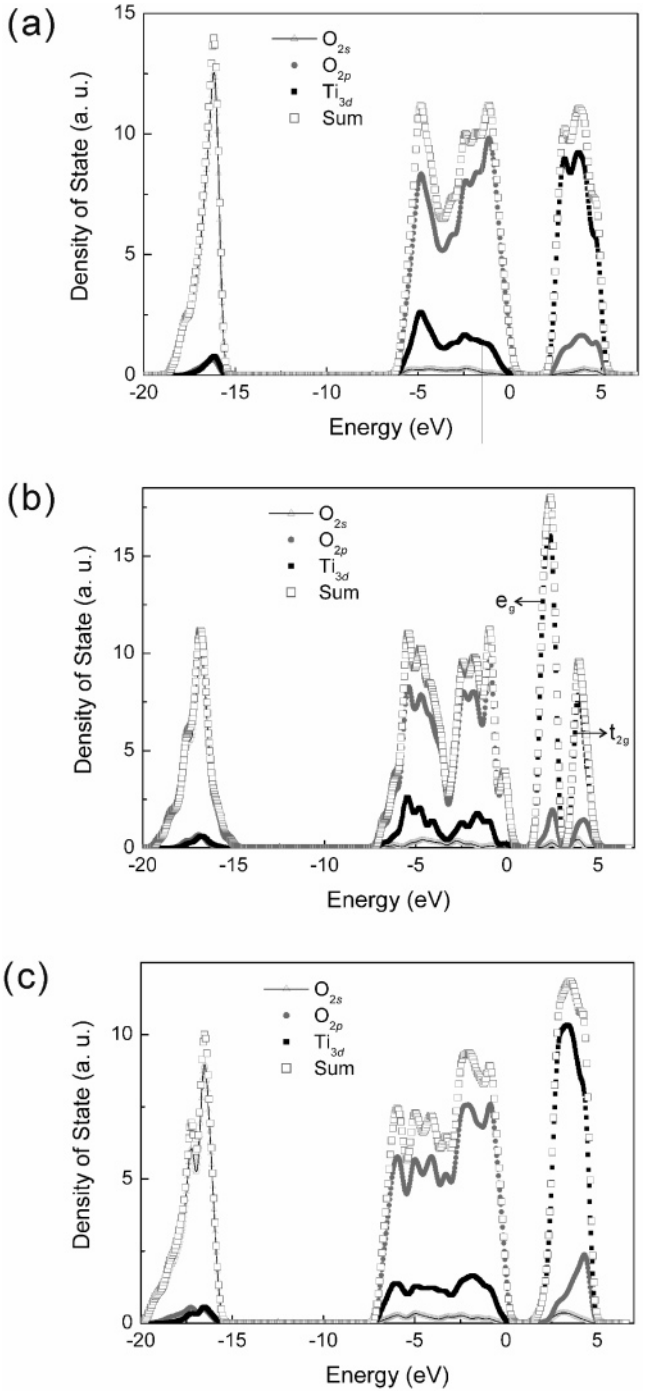

Figure 5. Total and partial DOS: (a) baddeleyite-, (b) fluorite-, (c) cotunnite-type TiO_2.

for this type of TiO_2. (We also conducted the energy band calculation of fluorite-type TiO_2 using a larger *k*-point mesh, i.e., $8 \times 8 \times 8$ instead of $4 \times 4 \times 4$. The band structure and band gap were not affected significantly by such an increase of the *k*-point mesh.) Figure 5b and Table 5 showed that the calculated upper VB and the lower O_{2s} are 7.54 and 4.18 eV in width, respectively, for fluorite-type TiO_2. The two bands are significantly wider for fluorite-type TiO_2 than those for the less dense polymorphs. However, the calculated gap between the O_{2s} valence states and the minimum of the CB for fluorite-type TiO_2 is 16.60 eV, considerably smaller than those for the TiO_2 polymorphs with a lower CN.

The electronic properties of cotunnite-type TiO_2 (Table 5) were calculated based on the theoretical and experimental lattice parameters listed in Table 3. The band structure (Figure 4c)

TABLE 6: Ti-O Bond Length and Average Ti−O Bond Length after Relaxation[a]

	Ti−O bond length (Å)	average Ti−O bond length (Å)	band gap (eV)
rutile	1.934 (4), 1.968 (2)	1.945	1.86
anatase	1.915 (4), 1.974(2)	1.935	2.13
α-PbO_2 type	1.862 (2), 1.938 (2), 2.067 (2)	1.956	2.62
baddeleyite	1.864, 1.934, 1.989, 1.999, 2.018, 2071, 2.148	2.003	2.15
fluorite	2.056 (8)	2.056	1.08
cotunnite	1.975, 1.984 (2), 2.016, 2.056, 2.127 (2), 2.342 (2)	2.106	1.72

[a] Numbers in parentheses indicate the number of this kind of bond. The energy band gaps are also compiled.

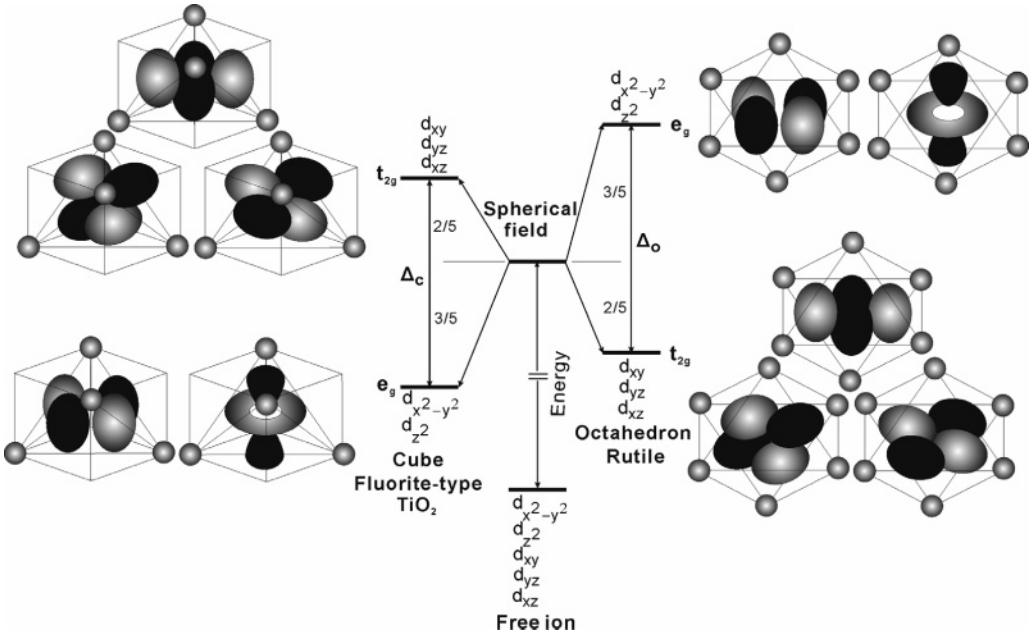

Figure 6. Orientation of the d orbitals with respect to the ligand positions and their crystal-field (CF) energies, i.e., CF splittings Δ_i in cubic octahedral (i = o) and cube (i = c) fields (after Figure 2 of ref. 43) for rutile and fluorite-type TiO_2, respectively.

and corresponding DOS/PDOS (Figure 5c) were shown representatively for the case using theoretical ambient lattice parameters. The cotunnite-type TiO_2 has a direct band gap of 1.72 eV (Figure 4c), and the upper VB and the lower O_{2s} are 6.94 and 3.64 eV in width, respectively (Figure 5c). The gap between the O_{2s} valence states and the minimum of the CB is 16.60 eV. An additional calculation using the experimental lattice parameters at high pressure (60 GPa) gives a direct band gap of 1.65 eV (Table 5).

IV. Discussion and Implications

Table 6 lists the averaged Ti−O bond lengths and band gaps of various TiO_2 polymorphs after relaxation. These properties are obtained with theoretical parameters at ambient pressure. The averaged Ti−O bond lengths turned out to be longer for the TiO_2 polymorphs with CN > 6 than those with CN = 6, i.e., rutile, anatase, and α-PbO_2-type TiO_2. In general, the increase of bond length between cation and anion may decrease the coupling constant and consequently decrease the band gap according to spectroscopic analysis of a set of tetrahedrally coordinated semiconductors.[42] The calculated band gap of the TiO_2 polymorphs, however, does not follow such a simple bond length−band gap correlation. In fact, the calculated bond length is longer for a α-PbO_2-type structure than those for rutile and anatase, and they are longer for cotunnite than those for fluorite, but the calculated band gap follows a reverse trend. As an alternative to bond length, we suggest that crystal symmetry and CN affect the extent of mixing of the Ti_{3d} and O_{2p} orbitals, and hence the band gap of the TiO_2 polymorphs is addressed below.

Table 1 lists the crystal symmetry of various TiO_2 polymorphs. The ambient phases rutile and anatase are tetragonal, which has a higher symmetry than the orthorhombic α-PbO_2 or cotunnite types of structures but lower than the cubic fluorite-type structure. (The symmetry order of crystal systems is monoclinic < orthorhombic < tetragonal < cubic.) Thus, the band gap correlates apparently with the crystal symmetry. In fact, the fluorite-type structure has the highest crystal symmetry and hence the narrowest band gap among the TiO_2 polymorphs. The underlying factors are the CN and symmetry of the polyhedra in the crystal that affect the extent of mixing of the Ti_{3d} and O_{2p} orbitals.

For the fluorite-type TiO_2 having the Ti atoms in 8-fold coordination with the oxygen atoms (i.e., a perfect octahedral symmetry (O_h) around the Ti atoms), the bottom of the conduction band, just above the Fermi level, is primarily determined by the unoccupied Ti d states and the O orbitals with p character (Figure 5b). An independent calculation using the APW method[41] showed detailed crystal-field splitting/degeneration of e_g and t_{2g} states of the Ti 3d electrons (cf. Figures 3b and 5 of ref 41) due to the O_h ($m3m$) symmetry of the Ti sites. (The two groups of unoccupied orbitals recall the crystal-field splitting of the Ti 3d states of the $[TiO_8]^{-12}$ ion into the triply degenerate t_{2g} and doubly degenerate e_g states.[41])

The present calculations of the density of states further indicated that the density of the conduction band is higher for fluorite (Figure 5b) than those for baddeleyite (Figure 5a) and cotunnite types of structures (Figure 5c) with distorted TiO_7 and TiO_9 species, respectively. This implies that CN and symmetry of the polyhedra are important factors of the band gap for the TiO_2 polymorphs. In a cube coordination (O_h) the d_{xy}, d_{yz}, and d_{xz} orbitals point toward the edges of the cube (distance to ligand $a/2$) and the $d_{x^2-y^2}$ and d_{z^2} orbitals (i.e., t_{2g}) toward the cube faces (at the distance $a\sqrt{2}/2$) (Figure 6). Hence, as compared to a spherical field, the d_{xy}, d_{yz}, and d_{xz} will be increased in energy and hence destabilized, while the $d_{x^2-y^2}$ and d_{z^2} orbitals (i.e., e_g) will be lowered in energy and hence stabilized (cf. Figure 2 of ref 43). The lowering of e_g in the CB is supported by the calculated band structure (Figure 4b) and DOS in Figure 5b. The band of Ti-derived conduction states is likely split in two; the lowering of one of the two subbands causes a reduction of the gap for fluorite-type TiO_2.[41] In the case of another cubic TiO_2 with a hypothetical pyrite structure, the metal site symmetry is lowered to C_{3i} (S_6).[41] Therefore, there is an additional splitting of the Ti 3d orbitals with resultant calculated direct band gap of 1.81 eV and an indirect band gap of 1.44 eV for the pyrite structure.[41]

The band gap of a semiconductor is the minimum energy required to excite an electron from the VB to CB. Conventional TiO_2 photocatalyst was composed of rutile, anatase, or their mixtures. The two ambient TiO_2 polymorphs have band gaps in the range 3.0−3.2 eV and hence respond only to ultraviolet rays. TiO_2 particles with smaller band gaps responsive to visible light are expected to have new applications.[44] In the present calculation, the fluorite-type TiO_2 has the narrowest band gap (1.08 eV) among the TiO_2 polymorphs. By the systematic underestimation of calculation being taken into account, the real band gap for the fluorite-type TiO_2 should be larger than 1.08 eV. If the theoretical−experimental difference 1.1 eV for rutile or anatase is applied to this case, then the real band gap of fluorite-type TiO_2 is 2.18 eV. (The LDA band-gap underestimation of TiO_2 with fluorite and a hypothetical pyrite structure has been treated through a scissor operator,[45] whereby the empty and occupied bands are displaced relative to each other by a rigid shift.[41] They used a band-gap shift of 1.12 eV to match the experimental band gap of rutile. By doing this, one has assumed that the amount of the band-gap underestimation in rutile or anatase is very similar to that of the cubic TiO_2 polymorphs.)

A band gap of 2.18 eV corresponds to a wavelength 570 nm within the visible light range, although not necessarily specified as green by simply relying on the DFT-LDA results. According to the calculated imaginary part of the dielectric function, the fundamental absorption edge for fluorite-type TiO_2 occurs at 1.82 eV, resulting from transitions between the topmost VB and the bottom of the CB.[41] Therefore, fluorite-type TiO_2 may be very important in the future design of photocatalysts responsive to visible light. The cubic TiO_2 was able to retain ambient pressure by the laser ablation condensation route (cf. Figure 2 of ref 32). This cubic phase is likely fluorite-type because of its martensitic transformation into a baddeleyite-type structure.[32] The fluorite-type TiO_2 was also synthesized by static compression of anatase at a pressure of 48 GPa and temperatures between 1900 and 2100 K as indicated by X-ray diffraction followed by decompression at ambient temperatures (unpublished results cited in ref 41). Future pursuit of this type of TiO_2 as a visible-light-responsive photocatalyst is thus promising.

V. Concluding Remarks

Density functional theory and the common LDA were used to calculate the geometrical parameters, electronic band gaps, and the densities of states for various dense TiO_2 polymorphs, which were known to exist in nature or have been synthesized. The fluorite phase with the highest crystal symmetry turned out to have the narrowest band gap 1.08 eV, or 2.18 eV after underestimation correction, due to TiO_8 species in favorable of the mixing of Ti_{3d} and O_{2p} orbitals. An independent LDA calculation further indicated that the fundamental absorption edge for fluorite-type TiO_2 occurs at 1.82 eV, and the absorption efficiency in the wavelength range between 380 and 450 nm is much better for fluorite than those for rutile and a hypothetical cubic phase with pyrite structure.[41] Future experiments are required to see if the fluorite-type TiO_2 is indeed an important visible-light-responsive photocatalyst. It is also of interest to study theoretically or experimentally the absorption edges of the noncubic TiO_2 polymorphs as has been done theoretically for anatase TiO_2 showing the dichroism with certain dipole selection rules.[46]

Acknowledgment. This research was supported by the Center for Nanoscience and Nanotechnology at NSYSU and the National Science Council, Taiwan, under contract no. NSC92-2120-M110-001. We thank the anonymous reviewers for constructive comments and Claire Shen for reading the manuscript.

References and Notes

(1) Fujishima, A.; Honda, K. *Nature* **1972**, *37*, 238.
(2) Bard, A. J. *J. Phys. Chem.* **1982**, *86*, 172. Bard, A. J. *J. Photochem.* **1979**, *10*, 59. Bard, A. J. *Science* **1980**, *207*, 139.
(3) Schiavello, M. *Photocatalysis and Environment*; Kluwer Academic Publishers: Dordrecht, 1988.
(4) Cromer, D. T.; Herrington, K. *J. Am. Chem. Soc.* **1955**, *77*, 4708.
(5) Baur, W. H. *Acta Crystallogr.* **1961**, *14*, 214.
(6) Mo, S. D.; Ching, W. Y. *Phys. Rev. B* **1995**, *51*, 13023.
(7) Simons, P. Y.; Dachille, F. *Acta Crystallogr.* **1967**, *23*, 334.
(8) Sato, H.; Endo, S.; Sugiyama, M.; Kiewgawa, T.; Shimomura, O.; Kusaba, K. *Science* **1991**, *25*, 786.
(9) Endo, S.; Takenaka, H.; Arashi, H. In *High-Pressure Science and Technology*, Proceedings of the Joint International Association for Research and Advancement of High-Pressure Science and Technology and American Physical Society Topical Group on Shock Compression of Condensed Matter Conference, Colorado Springs, CO, June 28−July 2, 1993; Schmidt, S. C., Shaner, J. W., Samara, G. A., Ross, M., Eds.; American Institute of Physics: New York, 1994; p 371.
(10) Dewhurst, J. K.; Lowther, J. E. *Phys. Rev. B* **1996**, *54*, R3673.
(11) Dubrovinsky, L. S.; Dubrovinskaia, N. A.; Swamy, V.; Muscat, J.; Harrison, N. M.; Ahuja, R.; Holm, B.; Johansson, B. *Nature* **2001**, *410*, 653.
(12) Hwang, S. L.; Shen, P.; Chu, H. T.; Yui, T. F. *Science* **2000**, *288*, 321.
(13) Poumellec, B.; Durham, B. P.; Guo, G. Y. *J. Phys.: Condens. Matter* **1991**, *3*, 8195.
(14) Daude, N.; Gout, C.; Jouanin, L. *Phys. Rev. B* **1977**, *15*, 3229.
(15) Hagfeldt, A.; Siegbahn, H.; Lindquist, S. E.; Lunell, S. *Int. J. Quantum Chem.* **1992**, *44*, 477.
(16) Glassford, K. M.; Chelikowsky, J. R. *Phys. Rev. B* **1992**, *46*, 1284.
(17) Göpel, W.; Anderson, J. A.; Frankel, D.; Jaehnig, M.; Phillips, K.; Schäfer, J. A.; Rocker, G. *Surf. Sci.* **1984**, *139*, 333.
(18) Tsutsumi, K.; Aita, O.; Ichikawa, K. *Phys. Rev. B* **1977**, *15*, 4638.
(19) Veal, B. W.; Paulikas, A. P. *Phys. Rev. B* **1985**, *31*, 5399.
(20) Grunes, L. A.; Leapman, R. D.; Wilker, C. N.; Hoffman, R.; Kunz, A. B. *Phys. Rev. B* **1982**, *25*, 7157.
(21) Knotek, M. L.; Feibelman, P. J. *Phys. Rev. Lett.* **1978**, *49*, 964.
(22) Vanderbilt, D. *Phys. Rev. B* **1990**, *41*, 7892.
(23) Payne, M. C.; Teter, M. P.; Allen, D. C.; Arias, T. A.; Joannopoulos, J. D. *Rev. Mod. Phys.* **1992**, *64*, 1045.
(24) Burdett, J. K.; Hughbanks, T.; Miller, G. J.; Richardson, J. W.; Smith, J. V., Jr.; Smith, J. V. *J. Am. Chem. Soc.* **1987**, *109*, 3639.
(25) Mikami, M.; Nakamura, S.; Kitao, O.; Arakawa, H.; Gonze, X. *Jpn. J. Appl. Phys.* **2000**, *39*, L847.

(26) Ramammoorthy, M.; Vanderbilt, D.; King-Smith, R. D. *Phys. Rev. B* **1994**, *49*, 16721.
(27) Lazzeri, M.; Vittadini, A.; Selloni, A. *Phys. Rev. B* **2001**, *63*, 155409.
(28) Muscat, J.; Swamy, V.; Harrison, N. M. *Phys. Rev. B* **2002**, *65*, 224112.
(29) Gerward, L.; Olsen, J. S. *J. Appl. Crystallogr.* **1997**, *30*, 259.
(30) Chen, S. Y.; Shen, P. *Phys. Rev. Lett.* **2002**, *89*, 096106.
(31) Milman, V. *Properties of Complex Inorganic Solids*; Plenum Press: New York, 1997.
(32) Chen, S. Y.; Shen, P. *Jpn. J. Appl. Phys.* **2004**, *43*, 1519.
(33) Pascual, J.; Camassel, J.; Mathieu, H. *Phys. Rev. Lett.* **1977**, *39*, 1490. Pascual, J.; Camassel, J.; Mathieu, H. *Phys. Rev. B* **1978**, *18*, 5606.
(34) Arntz, F.; Yacoby, Y. *Phys. Rev. Lett.* **1966**, *17*, 857.
(35) Tang, H.; Berger, H.; Schmid, P. E.; Lévy, F.; Burri, G. *Solid State Commun.* **1993**, *87*, 847.
(36) Kowlczyk, S. P.; Mcfeely, F. R.; Ley, L.; Gritsyna, V. T.; Schirley, D. A. *Solid State Commun.* **1977**, *23*, 161.
(37) Fisher, D. W. *Phys. Rev. B* **1972**, *5*, 4219.
(38) Sanjinés, R.; Tang, H.; Berger, H.; Gozzo, F.; Margaritondo, G.; Lévy, F. *J. Appl. Phys.* **1994**, *75*, 2945.
(39) Dreizler, R. M.; Gross, E. K. U. *Density Functional Theory: An Approach to the Quantum Many-Body Problem*; Springer-Verlag: Berlin, 1990.
(40) Sorantin, P. I.; Schwarz, K. *Inorg. Chem.* **1992**, *31*, 567.
(41) Mattesini, M.; de Almeida, J. S.; Dubrovinsky, L.; Dubrovinskaia, N.; Johansson, B.; Ahuja, R. *Phys. Rev. B* **2004**, *70*, 115101.
(42) Phillips, J. C.; Van Vechten, J. A. *Phys. Rev. B* **1970**, *2*, 2147.
(43) Wildner, M.; Andrut, M.; Rudowicz, C. Z. *Spectroscopic Methods in Mineralogy*; European Mineralogical Union Notes in Mineralogy; Beran, A., Libowitzky, E., Eds.; Eötvös University Press: Budapest, Hungary, 2004; Vol. 6, Chapter 3, pp 93−143.
(44) Asahi, R.; Morikawa, T.; Ohwaki, T.; Aoki, K.; Taga, Y. *Science* **2001**, *293*, 269.
(45) Del Sole, R.; Girlanda, R. *Phys. Rev. B* **1993**, *48*, 11789.
(46) Asahi, R.; Taga, Y.; Mannstadt, W.; Freeman, A. J. *Phys. Rev. B* **2000**, *61*, 7459.